Quantifying compressible groundwater storage by combining cross-hole seismic surveys and head response to atmospheric tides

Gabriel C. Rau[1,2*], R. Ian Acworth[1,2], Landon J. S. Halloran[3], Wendy A. Timms[1,4], Mark O. Cuthbert[1,5]

[1]Connected Waters Initiative Research Centre (CWI), UNSW Sydney, Australia
[2]Water Research Laboratory (WRL), School of Civil and Environmental Engineering, UNSW Sydney, Australia
[3]Centre d'Hydrogéologie et de Géothermie (CHYN), Université de Neuchâtel, Switzerland
[4]School of Mining Engineering, UNSW Sydney, Australia
[5]School of Earth and Ocean Sciences, Cardiff University, Cardiff, United Kingdom

---

Key Points:

- Cross-hole seismic surveys and tidal head analysis can be combined to improve estimates of specific storage
- We have developed an upper bound for specific storage for unconsolidated materials with low adsorbed water fractions
- Derived values of specific storage larger than this upper bound imply inappropriate use of oversimplified hydrogeological conceptual models

---

*Water Research Laboratory, 110 King Street, Manly Vale NSW 2093, Australia

Corresponding author: Gabriel C. Rau (gabriel.rau@unsw.edu.au)

Abstract

Groundwater specific storage varies by orders of magnitude, is difficult to quantify, and prone to significant uncertainty. Estimating specific storage using aquifer testing is hampered by the non-uniqueness in the inversion of head data and the assumptions of the underlying conceptual model. We revisit confined poroelastic theory and reveal that the uniaxial specific storage can be calculated mainly from undrained poroelastic properties, namely uniaxial bulk modulus, loading efficiency and the *Biot-Willis* coefficient. In addition, literature estimates of the solid-grain compressibility enables quantification of subsurface poroelastic parameters using field techniques such as cross-hole seismic surveys and loading efficiency from the groundwater responses to atmospheric tides. We quantify and compare specific storage depth profiles for two field sites, one with deep aeolian sands and another with smectitic clays. Our new results require bulk density and agree well when compared to previous approaches that rely on porosity estimates. While water in clays responds to stress, detailed sediment characterization from a core illustrates that the majority of water is adsorbed onto minerals leaving only a small fraction free to drain. This, in conjunction with a thorough analysis using our new method, demonstrates that specific storage has a physical upper limit of $\lessapprox 1.3 \cdot 10^{-5}\, m^{-1}$. Consequently, if larger values are derived using aquifer tests analysis then the conceptual model that has been used needs re-appraisal (e.g., by including vertical leakage). Our method can be used to improve confined groundwater storage estimates and refine the conceptual models used to interpret hydraulic aquifer tests.

1 Introduction

Groundwater compressible storage has always been difficult to quantify with high certainty using field techniques. Pumping-test analysis can be used to derive the aquifer properties of transmissivity and storage for a confined aquifer, but the degree of accuracy achieved for storage is often less than that achieved for transmissivity [*Kruseman and de Ridder*, 1990]. Theoretical approaches [*Narasimhan*, 1979; *Narasimhan and Kanehiro*, 1980] shed some light on the concept of storage and led to further discussion [*Bredehoeft and Cooley*, 1983; *Narasimhan*, 1983], with *Hsieh et al.* [1988] concluding that it was only possible to estimate S_s to within ± 50 %. *Wang* [2000] reviewed the field of poroelasticity with applications from the geotechnical field and from hydrogeology. Specific storage is now recognized as one of the fundamental coefficients of poroelastic theory [*Green and Wang*, 1990], along with Young's modulus (E), the shear modulus (G), and Poisson's Ratio (μ). Its value can also vary with time due to human activity [*David et al.*, 2017].The subject area has been overly complicated by the use of a variety of definitions and specialized terminology.

The response of a groundwater system to pumping, such as a decrease of hydraulic head or the development of land subsidence in aquitards, can only be predicted to any degree of accuracy if compressible storage properties are known at some reasonable vertical resolution [*Alley et al.*, 2002]. Although aquifer test analysis, taking account of leakage factors [*Hantush*, 1960, 1967a,b] and using multiple piezometers [*Kruseman and de Ridder*, 1990], may permit the estimation of storage properties at multiple depths, in practice these methods are not used due to the time and expense required to establish a site and the great length of time (weeks to months) required to obtain representative responses in lower hydraulic conductivity layers. Traditionally, characterization at $\lesssim$1 m scale could be achieved through expensive sediment coring using sophisticated drilling equipment and laboratory assessment, but the validity of laboratory measurements over in-situ measurements has also been questioned [*Clayton*, 2011]. The accelerating depletion of global groundwater resources [*Wada et al.*, 2013; *Gleeson et al.*, 2012] necessitates development of accurate and low-cost methods to routinely establish profiles of specific storage so that the accuracy of predicted drawdowns and aquitard settlement can be assessed.

Acworth et al. [2016a] described a new method to quantify *in situ* barometric efficiency (BE) using the hydraulic head response to atmospheric and earth tides. We refer to this as "tidal analysis" from here onwards. Data for three different BE values across the possible range from 0 to 1.0 [*Acworth et al.*, 2016a] and for a profile of ten different depths at a single site were described [*Acworth et al.*, 2017]. *Acworth et al.* [2017] used the BE analysis to predict specific storage using the formulation of *Jacob* [1940]. However, *Van Der Kamp and Gale* [1983] and *Domenico* [1983] noted (independently) that the approach of *Jacob* [1940] was based on a one-dimensional analysis that neglects the possibility of horizontal movement and also assumes that the compressibility of individual grains is insignificant. *Van Der Kamp and Gale* [1983] proposed a more extensive analysis that required consideration of the compressibility of individual components of the material (β_s) and also whether the elastic coefficients used represented drained or undrained systems. Their analysis requires further data on the elastic properties, including the bulk modulus (K), the shear modulus (G), and Poisson's Ratio (μ) of the material. They noted that estimation of specific storage would be possible if these parameters were available. *Wang* [2000] provides a comprehensive overview of the theory of poroelasticity.

The cross-hole seismic method is well established in the geotechnical industry [*Mathews et al.*, 1994] where it is routinely used to determine profiles of Poisson's ratio (μ), shear modulus (G), and bulk modulus (K). It is a recommended investigation technique (ASTM Method D 4428/D 4428M) when carrying out design work in unconsolidated materials for foundation or tunneling design. The methodology has changed little from early work by *Davis and Taylor-Smith* [1980]; *Davis* [1989]. Despite the success and essential simplicity of the method, application to inform groundwater resource investigation appears limited [*Clayton*, 2011; *Crice*, 2011]. The cross-hole seismic method presents an opportunity to measure the variation of elastic moduli over depth. A complete profile at any vertical interval ($\lesssim$1 m, or less) is possible, allowing for realistic visualization of actual lithological variation of these moduli with depth. In addition, as the testing is of the ground between two boreholes, it is completely *in situ*, undrained and not subject to the inaccuracies due to sampling, sample recovery and stress changes before laboratory testing.

We present a new method to quantify profiles of specific storage in unconsolidated formations *in-situ* using a rigorous interpretation of poroelastic theory [*Van Der Kamp and Gale*, 1983; *Green and Wang*, 1990; *Wang*, 2000]. We combine loading efficiency derived from groundwater response to atmospheric tides in piezometers at multiple depths with elastic parameters derived from cross-hole seismic surveys. This interpretation is further strengthened by comparison with detailed laboratory data on formation water content and bulk density, derived from previously reported measurements on core material data previously reported [*Acworth et al.*, 2015]. Two sites with contrasting lithology, representing the end members of sand and clay dominated deposits, illustrate the usefulness of combining two geophysical techniques to provide reasonable bounds for compressible subsurface properties and demonstrate its implications for groundwater resource investigations.

2 Methodology

2.1 Poroelastic drained and undrained terminology in hydrogeology

Quantifying specific storage relies on the assumption that subsurface poroelasticity is linear. This has seen separate development in the areas of geomechanics, petroleum engineering and hydrogeology [*Wang*, 2000] that has caused a wide variety of definition and terminology. For reference, definitions of all variables used in this paper are listed in the Appendix (Table 2). In our analysis it is assumed that the subsurface system remains saturated and confined at all times.

The elastic coefficients involved in poroelastic coupling vary depending upon the time taken for a load to be applied and stress to dissipate [*Domenico and Schwartz*, 1997; *Wang*, 2000]. While two end-member conditions, undrained and drained, can be distinguished, it should be recognised that real field conditions may exist anywhere on the continuum between these end members depending on the relationship between the timescale of the applied stress changes, the hydraulic properties of the formation, and the distance to hydraulic boundaries. First, for rapid loading, as occurs with the passage of a seismic wave or the response to atmospheric tides at sub-daily frequency, there may be insufficient time for water to flow in response to the increased stress and pore pressure. Therefore, the loading occurs at constant mass ($d\zeta/dt = 0$ where ζ is the mass of fluid) and poroelastic coefficients represent *undrained* conditions. Second, and by contrast, if the loading occurs slowly and fluid has the opportunity to redistribute, the loading occurs at constant pore pressure ($dp/dt = 0$ where p is pore pressure) and represents *drained* conditions. In this work undrained parameters are explicitly denoted with the superscript u, drained parameters have no subscript, or (u) if a relationship can be used interchangeably for undrained and drained values. Note here that the term *drained* should not be confused with the interpretation that subsurface pores are drained of water, i.e. when the hydraulic head in a confined aquifer is lowered below the confining layer causing unconfined conditions, as is a common interpretation in hydrogeology. In our analysis it is assumed that the subsurface system remains saturated and confined at all times.

2.2 Subsurface poroelastic coefficients

Over the small range of pressure changes caused by tides and acoustic pulses, we assume that the matrix exhibits a perfectly elastic (i.e., *Hookean*) response. If such a material is subjected to a uniaxial compression or tension, a linear relationship exists between the applied stress σ and the resulting strain ϵ expressed as

$$\sigma = E^{(u)}\epsilon, \tag{1}$$

where E is a constant of proportionality known as *Young's Modulus*. The value of the strain ϵ is the ratio of the change in line length in its deformed state l_f to its initial state l_o

$$\epsilon = \frac{l_f - l_o}{l_o} = \frac{\Delta l}{l_o}. \tag{2}$$

If a *Hookean* solid is subject to uniaxial compression it will shorten in the direction of compression and expand in the plane at right angles to the direction of compression. If $\epsilon_{\parallel}$ represents the shortening in the direction of compression and $\epsilon_{\perp}$ represents the expansion in the plane at right angles to the compression, then the ratio of these two quantities is referred to as *Poisson's Ratio*

$$\mu^{(u)} = \frac{\epsilon_{\parallel}}{\epsilon_{\perp}} \leq 0.5. \tag{3}$$

A solid can also be deformed by means of a shear causing shear strain (ϵ) in response to the shear stress (σ). The ratio of these quantities is the shear (or rigidity) modulus

$$G = \frac{\sigma}{\epsilon}. \tag{4}$$

The shear modulus G is related to the Young's modulus E and Poisson's ratio μ by

$$G = \frac{E^{(u)}}{2(1+\mu^{(u)})}. \tag{5}$$

In an isotropic material subject to a change in pressure, a change in volume will occur. This is described by the *bulk modulus*:

$$K = -V\frac{dp}{dV} = \rho\frac{dp}{d\rho}, \tag{6}$$

where p is pressure, V is volume and ρ is material density. Further relationships for K are

$$K_{(s)}^{(u)} = G\frac{2\left(1+\mu_{(s)}^{(u)}\right)}{3\left(1-2\mu_{(s)}^{(u)}\right)} = \frac{E_{(s)}^{(u)}}{3\left(1-2\mu_{(s)}^{(u)}\right)}. \tag{7}$$

Note that these relationships apply for solid materials (indicated as (s)) as well as interchangeably for drained or undrained (indicated as (u)) conditions, with exception of the shear modulus G, which remains the same [*Wang*, 2000]. In the case of a homogeneous, isotropic, elastic materials, values for any two of the shear modulus G, Young's modulus E, bulk modulus K, or Poisson's ratio μ (or, additionally, the longitudinal modulus or Lamé's first parameter) are sufficient to define the remaining parameters for drained or undrained conditions [*Wang*, 2000].

2.3 Confined groundwater storage in a poroelastic formation

Wang [2000] provides a detailed analysis of poroelastic theory for both drained and undrained conditions, and *Van Der Kamp and Gale* [1983] develop expressions for the analysis of atmospheric and Earth tides, the expression of which in groundwater level time-series are normally considered as undrained phenomena. The developments build on the coupled equations for stress and pore pressure derived by *Biot* [1941] for very small deformations, typical of those that occur with the passage of seismic waves or in response to atmospheric tides. In the most general case, it is necessary to consider a fully deformable medium in which all components are compressible. Besides the bulk formation compressibility $\beta = 1/K$, which is the reciprocal of the bulk modulus $K = 1/\beta$, two more components require consideration. The water compressibility:

$$\beta_w = \frac{1}{K_w} \approx 4.58 \cdot 10^{-10}\, Pa^{-1}. \tag{8}$$

The solid grain (or unjacketed) compressibility

$$\beta_s = \frac{1}{K_s} \tag{9}$$

assumes homogeneous solids and is not well defined for mixtures of different grain types [*Wang*, 2000].

The volume of water displaced from a sediment is always less than the change in bulk volume whenever grain compressibility is included [*Domenico and Schwartz*, 1997]. To take account of this change, the *Biot-Willis* coefficient is used [*Biot*, 1941; *Wang*, 2000]

$$\alpha = 1 - \frac{\beta_s}{\beta} = 1 - \frac{K}{K_s}. \tag{10}$$

Note that if $\beta_s \ll \beta$ then there is relatively little, if any, change in volume of the grains when compared to the total volume change and therefore $\alpha \to 1$.

Van Der Kamp and Gale [1983] and *Green and Wang* [1990] presented a comprehensive relationship for specific storage that assumes only uniaxial (vertical) deformation (zero horizontal stress) and includes solid grain compressibility:

$$S_s = \rho_w g \left[\left(\frac{1}{K} - \frac{1}{K_s} \right)(1-\lambda) + \theta \left(\frac{1}{K_w} - \frac{1}{K_s} \right) \right], \tag{11}$$

where the density of water $\rho_w = 998\, kg/m^3$, the gravitational constant is $g = 9.81\, m/s^2$, θ is total porosity, and

$$\lambda = \alpha \frac{2}{3} \frac{(1-2\mu)}{(1-\mu)} = \alpha \frac{4G}{3K_v}. \tag{12}$$

Here, K_v is the drained vertical (or constrained) bulk modulus and expressed as [*Green and Wang*, 1990; *Wang*, 2000]

$$\frac{1}{K_v^{(u)}} = \beta_v^{(u)} = \frac{1+\mu^{(u)}}{3K^{(u)}\left(1-\mu^{(u)}\right)} = \left(K^{(u)} + \frac{4}{3}G \right)^{-1}. \tag{13}$$

If the solids are incompressible ($\beta_s = 1/K_s \rightarrow 0$) then Equation 11 reduces to the well-known formulation [*Jacob*, 1940; *Cooper*, 1966]

$$S_s = \rho_w g \left(\frac{1}{K_v} + \frac{\theta}{K_w} \right) = \rho_w g(\beta_v + \theta\beta_w), \tag{14}$$

We note that if $\mu^{(u)} = 0.5$ then it can be seen from Equation 13 that $K_v^{(u)} = K^{(u)}$. Note however, that this will only be the case for very unconsolidated silts or clays.

To summarize, specific storage values derived from Equations 11 and 14 represent vertical and isotropic stress only and are therefore smaller compared to the case where horizontal stress and strain is allowed to occur [*Wang*, 2000]. However, this is a reasonable and common assumption which suffices to represent the conditions encountered in a hydrogeological setting. For example, Equation 14 is widely used in hydrogeology [*Van Der Kamp and Gale*, 1983], particularly for the analysis of head measurements obtained from aquifer testing [e.g., *Kruseman and de Ridder*, 1990; *Verruijt*, 2016].

2.4 Elastic moduli from the propagation of seismic waves

Two fundamental wave motions can transmit energy through a formation. The first is a compressional, or primary wave (P-wave) whose speed is a function of the undrained uniaxial bulk modulus:

$$V_p = \sqrt{\frac{K_h^u}{\rho}} = \sqrt{\frac{K^u + \frac{4}{3}G}{\rho}}, \tag{15}$$

where K_h^u is the undrained bulk modulus [*Wang*, 2000, Page 60]. We have used the notation K_h^u to recognize that the wave front spreads out spherically from the source but is monitored in the horizontal plane. The geophone that is alligned in the horizontal direction and pointing to the source detects the primary wave arrival after the wave has progressed horizontally through the formation. Hence, the appropriate bulk modulus derived from this velocity (Equation 15) is an undrained uniaxial (horizontal) bulk modulus (K_h^u).

Due to the short distances between the source and receiver and the assumed homogeneity of unconsolidated deposits, we assume isotropic conditions and therefore that $K_v^u = K_h^u$. It is noted that it would be possible to investigate anisotropy in K^u by analysing the arrival times of the primary wave for the other two (one horizontal and one vertical) geophone components.

For sand and water mixtures, bulk density and total porosity of the formation are related through a simple volumetric mixing model [*Jury et al.*, 1991]

$$\rho = \rho_s(1 - \theta) + \rho_w\theta, \tag{16}$$

where ρ_s is the density of the solid phase (sand particles) generally assumed to be $2,650\ kg/m^3$, and the density of water $\rho_w \approx 998\ kg/m^3$.

The second wave motion is a shear wave (S-wave) that progresses through a material by motion normal to the direction of propagation:

$$V_s = \sqrt{\frac{G}{\rho}}. \tag{17}$$

Conveniently, the ratio of the compressional and shear wave velocities can be used to determine the undrained Poisson's ratio μ^u directly [*Davis and Taylor-Smith*, 1980]

$$\mu^u = \frac{V_p^2 - 2V_s^2}{2V_p^2 - 2V_s^2} \le 0.5. \tag{18}$$

Note that $V_s < V_p$.

2.5 Combining cross-hole seismic surveys and the groundwater response to atmospheric tides

Specific storage has previously been calculated from barometric efficiency (BE) estimates. *Acworth et al.* [2016a] developed an accurate method to quantify BE using the groundwater response to atmospheric tides when influences at frequency of 2 cpd. The method is given as

$$BE = \frac{S_2^{GW} + S_2^{ET}\cos(\Delta\phi)\frac{M_2^{GW}}{M_2^{ET}}}{S_2^{AT}}, \tag{19}$$

where S_2^{GW} is the amplitude of the hydraulic head, S_2^{ET} is the amplitude of the earth tide and S_2^{AT} the amplitude of the atmospheric tide; $\Delta\phi$ is the phase difference between the Earth tide and atmospheric drivers (both at 2 cpd frequency); M_2^{GW} is the amplitude of the hydraulic head and M_2^{ET} the amplitude of Earth tides at 1.9323 cpd frequency. The required amplitudes and phases can be obtained using the *Fourier* transform of atmospheric and head records which require a duration of ≥16 days with frequency of ≥12 samples per day [*Acworth et al.*, 2016a].

We note that an estimate of specific storage for a formation comprising incompressible grains can be made if the value of porosity is estimated [*Acworth et al.*, 2017]:

$$S_s = \rho_w g \beta_w \frac{\theta}{BE} \approx 4.484 \cdot 10^{-6} \frac{\theta}{BE}. \tag{20}$$

Estimating porosity can be problematic when dealing with fine-grained materials and, especially, smectitic clays where it is never clear what value of porosity exists due to the uncertainty regarding the volume of adsorbed water (i.e., hygroscopic water bound to the surface of the grains via molecular forces). This is due, in part, to the extreme values of surface area per volume characteristic of clays, which render the proportion of water molecules that are adsorbed rather than absorbed non-negligible.

In this paper, we develop a new method to quantify confined groundwater specific storage depth profiles *in situ* by combining cross-hole seismic measurements of elastic coefficients with the groundwater response to atmospheric tides. From *Wang* [2000] (Equations 3.84 and 3.81), a uniaxial specific storage equation can be derived as

$$S_s = \rho_w g \frac{\alpha}{K_v^u LE(1-\alpha LE)} \tag{21}$$

where LE is the uniaxial loading efficiency (or tidal efficiency), which can be calculated from BE as [*Domenico and Schwartz*, 1997; *Wang*, 2000]

$$LE = 1 - BE. \tag{22}$$

Equation 21 allows calculation of uniaxial specific storage mainly from undrained parameters which are readily measured using field techniques, e.g. seismics and tidal analysis. A discussion of α follows later.

Wang [2000] further shows that *Skempton's* coefficient can be calculated from undrained parameters as

$$B = 3LE\frac{1-\mu^u}{1+\mu^u} = \frac{1-K/K^u}{1-K/K_s} \tag{23}$$

which can be reformulated to arrive at a relationship between undrained and drained bulk modulus

$$K = \frac{K_s K^u (1-B)}{K_s - BK^u}. \tag{24}$$

To quantify specific storage using our new method of combining cross-hole seismic surveys and tidal analysis (Equation 21), K_v^u, G and μ^u are obtained from seismic velocities (Equations 15, 17 and 18) and LE stems from tidal analysis (Equations 19 and 22). To estimate the drained formation compressibility (24), B is calculated from seismically derived μ^u (Equation 18) and tidally derived LE (Equations 19 and 22), whereas K^u is calculated from seismically derived K_v^u and G (Equations 15 and 17). In both cases, values for K_s can be found in the literature and are discussed below.

2.6 Quantifying compressible groundwater storage at two field sites: Fine sands versus clays

We investigate and contrast the subsurface conditions at two field sites in Australia (Figure 1) with different lithology.

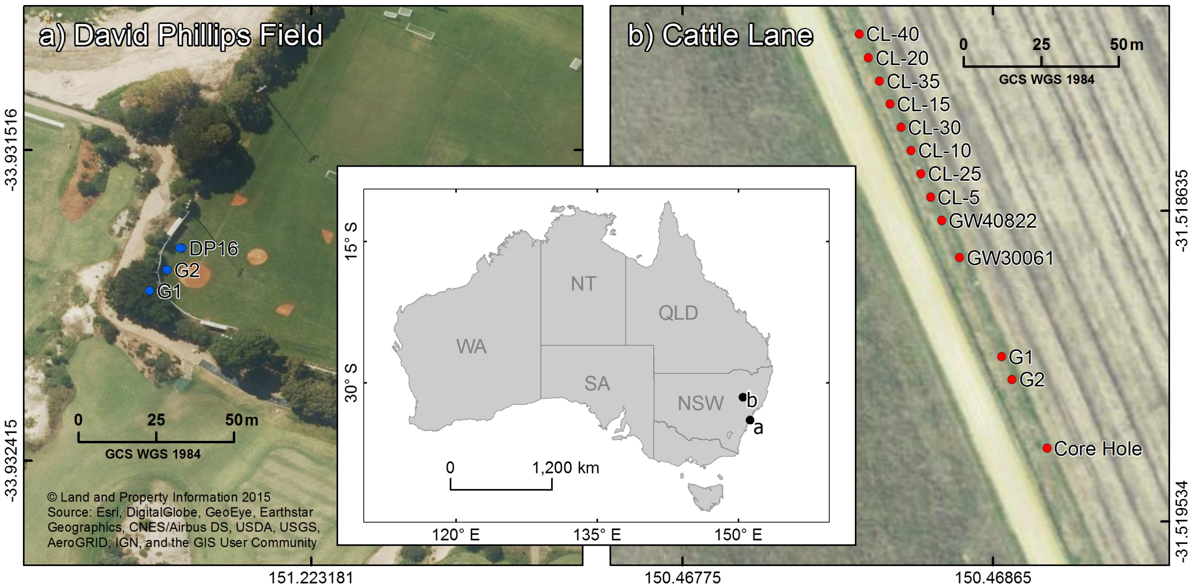

Figure 1. Map showing the locations of boreholes at David Phillips Field (aeolian sand) (a) and Cattle Lane (clay) (b) in New South Wales, Australia (inset map with locations).

2.6.1 Sand dominated site at David Philips Field

David Phillips Field is located on top of the Botany Sands Aquifer in Sydney, NSW (Figure 1a). During the last glacial epoch, sand has been blown from Botany Bay and now fills deep sided valleys in the Permo-Triassic Hawkesbury Sandstone [*Webb and Watson*, 1979; *Acworth and Jankowski*, 1993]. The sands provide an important water resource that, for a time, served Sydney. Webb and Watson report a very detailed pumping test at this site that determined There is an unconfined aquifer to approximately 7.5 m at the site, below which a thin layer of peat and silt acts to confine the underlying aquifer to approximately 17 m. Below this, a further silty sand separates a deeper confined aquifer [*Webb and Watson*, 1979]. The depth to the water table was approximately 7 m at the time of testing. *Acworth* [2007] reported the results of manometer board testing from the same field that included geophysical logs and detail on lithology. The sands are very well sorted with a median grain size of 0.3 mm and a typical porosity of $\theta \approx 0.35$ [*Acworth and Jankowski*, 1993].

Three bores were installed in the south-west corner of David Phillips Field (Figure 1a). The first bore penetrated Hawkesbury Sandstone (Permo-Triassic) at 31 m using a combination of rotary auger and and rotary mud drilling. The bore was completed at 36 m with 80 mm PVC casing. Cement gout was placed at the base of the sands and the formation above allowed to collapse back onto the PVC casing (Borehole G1 in Figure 1a). A second bore was installed using hollow-stem augers to a depth of 28 m (Borehole G2 in Figure 1a), while a third bore was installed to 16 m depth (DP16 in Figure 1a). Both these bores were completed using 50 mm PVC with a 1 m screen set at the base.

Water level data for the Botany Site at David Philips Field were measured in piezometer DP16. A Diver data logger was used with a sampling interval of 1 hour. The atmospheric pressure was compensated using the record from Sydney Airport (≈4 km from the field site). There is only a single value of barometric efficiency ($BE = 0.151$) available for David Phillips Field from Piezo-16 (Figure 1a).

2.6.2 Clay dominated site on the Liverpool Plains

The second field site, Cattle Lane, is located on the Liverpool Plains, NSW (Figure 1b). Deposition of clay derived from the nearby Liverpool Ranges has occurred onto the Liverpool Plains (south to the north). The saturated zone at this site is typically within a meter or two of the ground surface. Clay deposition has been dominant during drier periods, with silt and clay deposited during colder periods and gravels and sands during periods of higher rainfall. This sequence has been proven by coring ('Core Hole' on Figure 1a) to 31.5 m depth and the lithology is given by *Acworth et al.* [2015]. Note that the subsurface is very homogeneous in the horizontal direction (150 m between CL40 and the core hole, Figure 1) as determined by surface-based geophysics across the site [*Acworth et al.*, 2015].

To conduct the cross-hole seismic survey [*Crice*, 2011] at Cattle Lane, two boreholes were drilled to 40 m depth adjacent to the cored hole (G1 and G2 shown in Figure 1). The boreholes were lined with thin-walled PVC casing that was grouted in place using a weak cement/mud slurry forced out of the base of the casing and allowed to overflow back to the surface outside the casing, ensuring that no air gaps were present. Good continuity was achieved between the formation and the casing with no air gaps to ensure unrestricted passage of seismic waves.

Bulk densities were measured on the clay samples recovered from the core nose of the triple-tube core barrel [*Acworth et al.*, 2015] immediately after sample collection. Densities corresponding to the depths of the cross-hole measurements were calculated by interpolation of measurements at known depths. Samples were also dried and weighed to obtain total moisture and bulk density data (Table 1). Essential data for the core measurements at the site are presented in Table 1.

There are a A total of nine piezometers screened at 5 m intervals between 5 and 55 m depth exist at Cattle Lane. Water levels were measured in these piezometers using vented pressure transducers (LevelTroll, InSitu Inc, USA). We note that the subsurface processes at this site are relatively well understood and have been reported in a number of previous papers. For example, In prior studies, the lithology was sampled by obtaining minimally disturbed 100 mm core followed by extensive laboratory testing and analysis [*Acworth et al.*, 2015] and the barometric efficiency and degree of confinement over depth established [*Acworth et al.*, 2016a, 2017]. We extensively make use of this existing dataset in order to add context to the cross-hole seismic survey and further improve our understanding of the unconsolidated subsurface.

2.7 Cross-hole seismic survey procedure

At both sites, a seismic source (Ballard borehole shear wave source) was lowered into the borehole and clamped to the casing using an inflatable bladder expanded using air pressure.

Core Sample Depth z (m BGS)	**Water Content** θ (%)	**Natural Density** ρ (kg/m^3)	**Free-water Porosity** θ_{free} (%)	**Piezo Depth** z (m)	**BE** (-)
2.68	64.71	1659	0.015	5	0.010
4.35	31.25	1907	0.010	10	0.007
5.85	43.48	1926	0.007	15	0.032
7.35	46.43	1864	0.007	20	0.039
10.35	52.94	1721	0.007	25	0.042
11.85	47.37	1707	0.005	30	0.042
13.35	36.36	1997	0.020	35	0.059
14.85	58.57	1763	0.018	40	0.121
16.40	48.44	1664	0.018	55	0.138
17.35	47.37	1748	0.020		
19.35	52.38	1721	0.023		
20.85	55.56	1821	0.023		
22.35	45.45	1807	0.020		
23.85	52.63	1815	0.020		
26.85	36.17	1924	0.020		
28.35	34.29	1940	0.020		
29.85	44.99	1756	0.022		
31.35	25.00	2075	0.023		

Table 1. Depth profile of moisture content and density for core samples [*Acworth et al.*, 2015] and BE values from piezometers [*Acworth et al.*, 2017] at the Cattle Lane site. Note: Estimates of free-water porosity (θ_e) are based upon the analysis of density developed in Section 3.1.2. BGS = "below ground surface." BE = "barometric efficiency"

Upward and downward polarized shear waves were generated by either dropping a weight onto the clamped frame or pulling the weight upwards so that it struck the clamped frame. P-waves were generated by both upward and downward blows on the clamped frame. Seismograms were recorded using a submersible three-component geophone (Geostuff wall-lock geophone). The geophone had two horizotal and one vertical element and was locked in place using a mechanical arm (steel spring) that was activated from the surface. The horizontal components were configured so that one component was normal to the source bore and the second at right angles using an on-board magnetometer element to sense direction.

Seimograms were recorded by a multi-channel seismograph using image stacking to improve the signal-to-noise ratio. In general, six upward and six downward blows provided a clear indication of the shear wave arrival. Data was collected either at 0.5 m or 1.0 m intervals, but the station interval was arbitrary. Data collection required between 2 and 3 hours work. The distance between the shot and receiver bores at different depths was established by running borehole verticality logs (Geovista verticality sonde) in each bore. The verticality-distance relationships were combined to calculate the distance between the source and receiver at each required depth. Wave arrival times were estimated using the vertical component for the shear waves and the beginning of the phase difference between the upward and downward blows. Similarly, the compressional wave arrivals were estimated using the horizontally orientated geophones. Wave velocities were established using the horizontal distance between the sensors established from the verticality survey .

3 Results and Discussion

3.1 Combining cross-hole seismic surveys and tidal analysis reveals subsurface properties

Example primary and shear wave measurements are shown in Figure 2 to illustrate the data collected from the three-component geophones. The P-wave arrivals are noticeably in phase, whereas the S-wave arrivals are 180° apart. As the vertical component presents the clearest arrival time, it is used in the investigation of shear-wave anisotropy.

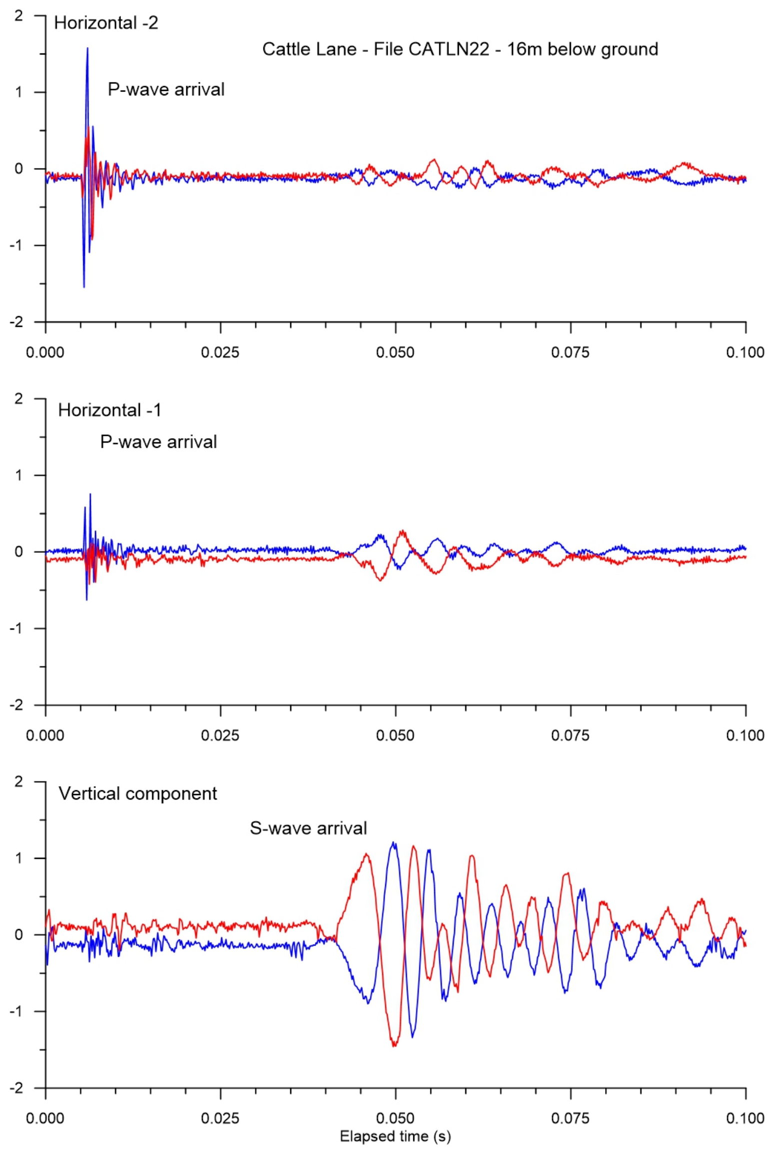

Figure 2. Example output from the three-component geophone showing the arrivals from upward (red) and downward (blue) polarities measured at 16 m BGS at Cattle Lane (Figure 1b).

We calculate the drained and undrained poroelastic parameters from undrained measurements using values for grain compressibility provided in the literature. Further, two different specific storage depth profiles are calculated and compared: (1) Equation 20: This approach assumes a porosity as well as incompressible grains ($K_s = 0$); (2) Equation 21: In this new method, the required parameters are obtained by combining cross-hole seismic surveys and tidal analysis. Here, it is noteworthy that the bulk density ρ is required instead of porosity. Further, the influence of compressible grains can be explored by taking K_s values from the literature. This mathematically constrains the poroelastic parameter space so that K values can be obtained from Equation 24.

3.1.1 Sand dominated site: David Phillips Field

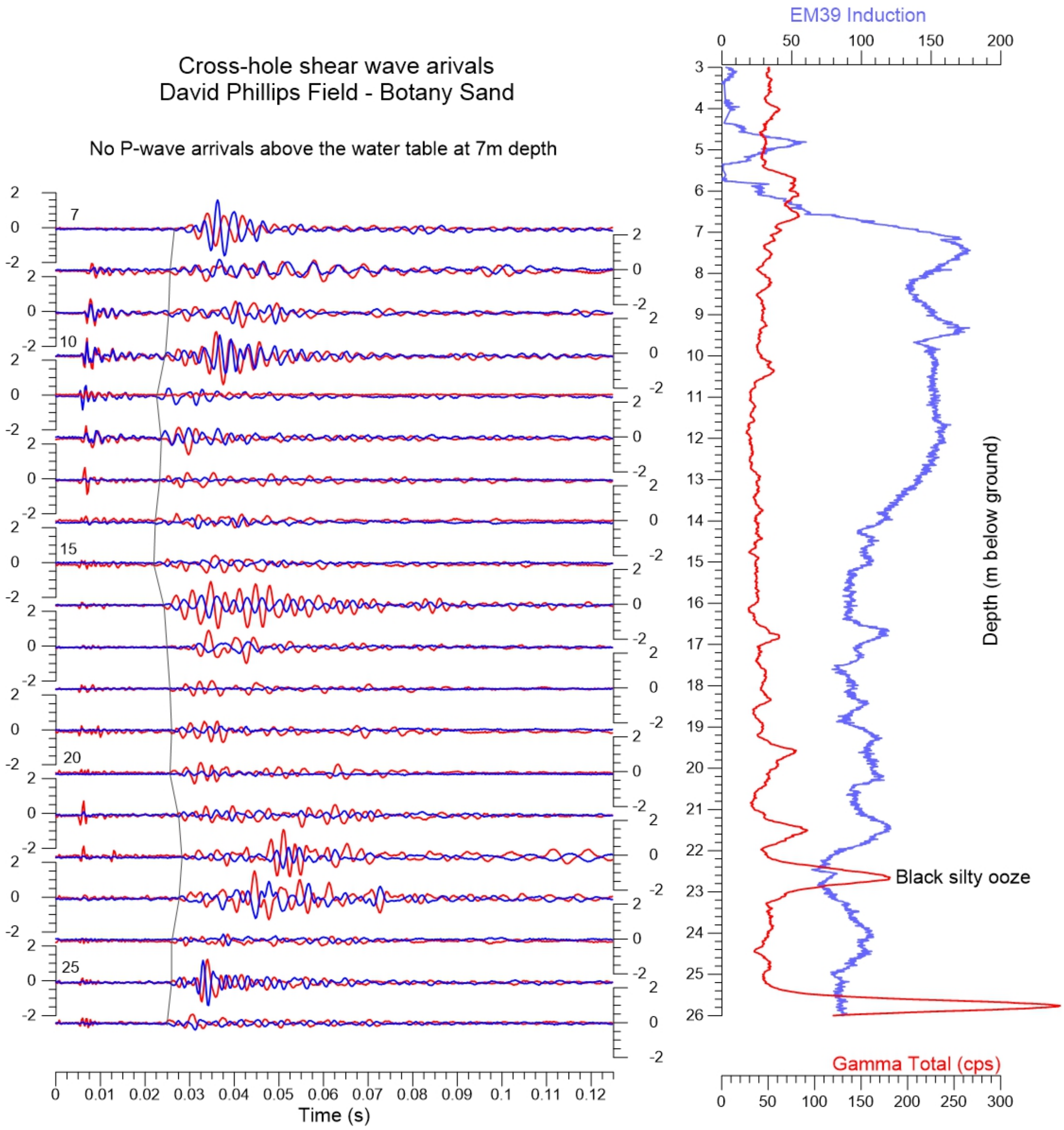

Figure 3. Profile of the vertical component cross-hole survey results from bore G2 at David Phillips Field (Figure 1a) vertically co-located with an EM39 induction and gamma depth survey.

The seismic waveforms (Figure 3) measured during the cross-hole survey at David Phillips Field are shown along with the gamma-ray activity and bulk electrical conductivity (EC) logs to provide a lithological comparison. The water level in the sands at the time of measurement was ~7 m below ground surface. Both *P*- and *S*-wave arrivals were detected above this depth. Elevated bulk EC levels between 7 m and 15 m represent contaminated groundwater moving laterally from an old waste fill and the elevated gamma-ray activity at 23 m is considered to be an old inter-dune wetland that may have trapped dust [*Acworth and Jorstad*, 2006].

The shear wave results for the David Phillips Field (Figure 3) indicate that there is significant variation in signal amplitude with depth, although the source signal was produced manually, i.e. by pulling up or letting the shear source weight drop down. This suggests that the shear wave amplitude could be used to indicate lithological variability. The sedimentary sequence at this site was examined during drilling to comprise uniform sands to 22 m depth with a black silty ooze at 23 m before a return to uniform sands. Samples were not kept as the sequence appeared so uniform.

Shear-wave amplitudes suggest that considerably greater variabilityis present that may indicate differences in consolidation or proto-soil development due to a break in sand accumulation. The sequence is undated although tree remains from approximately 30 m at a site in the sands 800 m to the southwest give an uncorrected radio-carbon date of ~30,000 BP. Variability in sediment accumulation rate and type would have occurred through the last glacial maximum at this site.

The results derived from the cross-hole survey at David Phillips Field are shown in Figure 4a (and presented in Table S1). In the absence of depth-specific information, a density of $\rho = 2,072\,kg/m^3$ was determined using Equation 16 with a total moisture content $\theta = 0.35$ [*Acworth and Jankowski*, 1993]. As a first approximation, porosity, density and loading efficiency were not considered to vary with depth. Fine-grained sands with thin beds of silt/clay at the site were reported by *Webb and Watson* [1979]. The barometric efficiency measured in the piezometer installed at 16 m (BE = 0.151) was used to calculate the loading efficiency ($LE = 0.849$, Equation 22).

Richardson et al. [2002] report a solid grain modulus for Ottawa Sand in the range of $30 \leq K_s \leq 50$ GPa using 95% confidence limits, which they consider to be consistent with values for polycrystalline quartz found in the literature ($36 \leq K_s \leq 40$ GPa) and also for glass beads. The Ottawa Sands had a fractional porosity of 0.373, a mean *P*-wave velocity of $1,775\,m/s$, a bulk density of $2,080\,kg/m^3$ and a grain density of 2,670 kg/m^3. As the physical properties of the Ottawa Sand sample closely match those from David Phillips Field, we have selected the mid point of the solid grain modulus range ($K_s = 42\,GPa$), which represents a $\beta_s \approx 2.632 \cdot 10^{-11}\,Pa^{-1}$, for our poroelastic analysis.

The results of the poroelastic calculations are summarized in Figure 4. Figures 4b-d show the calculated depth profiles for the poroelastic coefficients. Figure 4e compares the three specific storage estimates calculated using:

- Equation 20 (for the single value of LE at 16 m depth). This is the conventional analysis that is based upon *Jacob* [1940] and is implemented in *Acworth et al.* [2017];
- Equation 11 with values calculated for $K_s = 42\,GPa$ ($\alpha <$) as well as $K_s \rightarrow \infty$ ($\alpha = 1$). This is a fully developed poroelastic solution where knowledge of parameters are required, i.e. estimates for porosity, drained bulk modulus K, solid grain modulus K_s, and shear modulus G or Poisson ratio μ;
- Equation 21 with values calculated for $K_s = 42\,GPa$ ($\alpha <$) as well as $K_s \rightarrow \infty$ ($\alpha = 1$). This is the new poroelastic approach presented in this paper which requires density estimates.

We note the agreement between the three specific storage calculations (Figures 4e). The values of specific storage decrease from $S_s \approx 2 \cdot 10^{-5}\,m^{-1}$ to $S_s \approx 1.2 \cdot 10^{-5}\,m^{-1}$ over depth. We note also that bulk density and porosity are related (Equation 16), an observation that we will return to below.

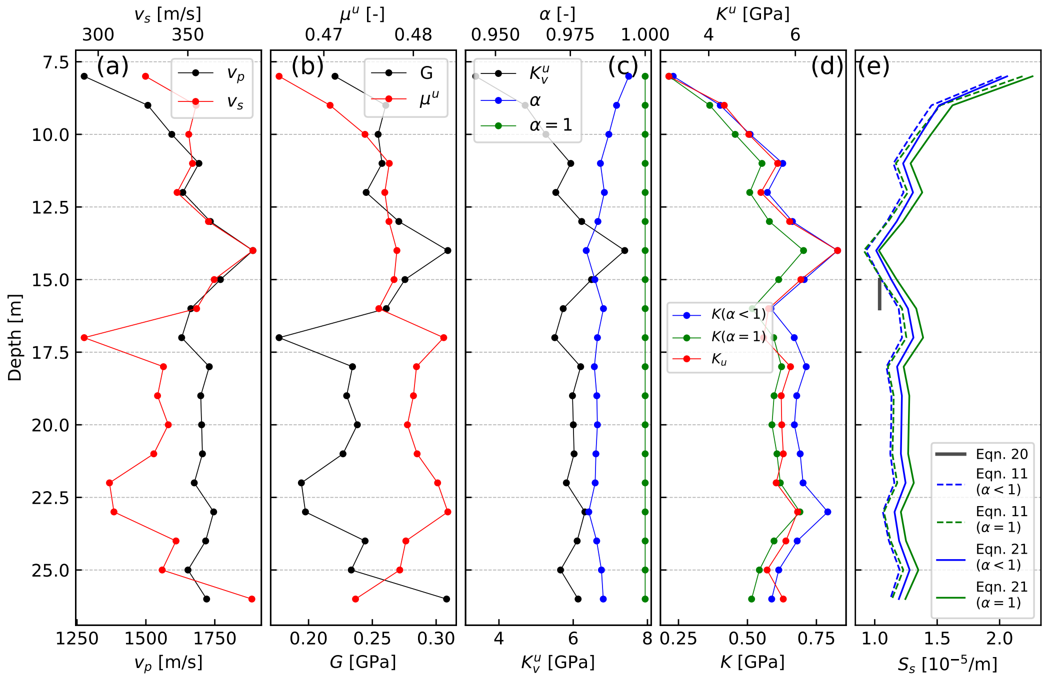

Figure 4. Results for the David Phillips Field Site (a) Primary and shear wave velocity data; (b) Undrained Poisson's Ratio and Shear modulus (c) *Biot-Willis* coefficient (α) and undrained (vertical) bulk modulus (K_v^u) (d) Drained (K) and undrained (K^u) bulk moduli (e) Specific storage estimates using parameter ranges as described in the text.

3.1.2 Clay dominated site: Cattle Lane

The seismic waveforms recorded during the cross-hole survey by the vertically orientated geophone at Cattle Lane are shown in Figure 5. The depth of each seismogram is arranged so that the zero amplitude is adjacent to the depth below ground level used for the geophysical logs. The associated seismic velocity analysis is presented in Table S2 of the Supplementary Information.

A detailed lithological characterization for this site has previously been published [*Acworth et al.*, 2015, 2016a] and provides physical data and observations that we draw upon for the poroelastic analysis in this work. S-wave variability was significantly higher at this site than at David Phillips Field. It is therefore assumed that the observed variability is a function of lithology and not a measurement artifact. The shear-wave data was collected to 38 m, a depth that correlates to an age of approximately 150 ka [*Acworth et al.*, 2015] and covers the start of the penultimate glacial, the interglacial and the last glacial stages of the Ice Age.

It is not the intention to fully interpret the correlations between the shear-wave arrivals and waveforms but to note that there appear to be relationships between shear waveforms and the past climate variations that cause the different lithologiesobserved. For example, the clear change in shear waveform at 14 and 15 m depth (much reduced amplitude and lower frequency) shown in Figure 5 correlates with the depth at which *Acworth et al.* [2015] ob-

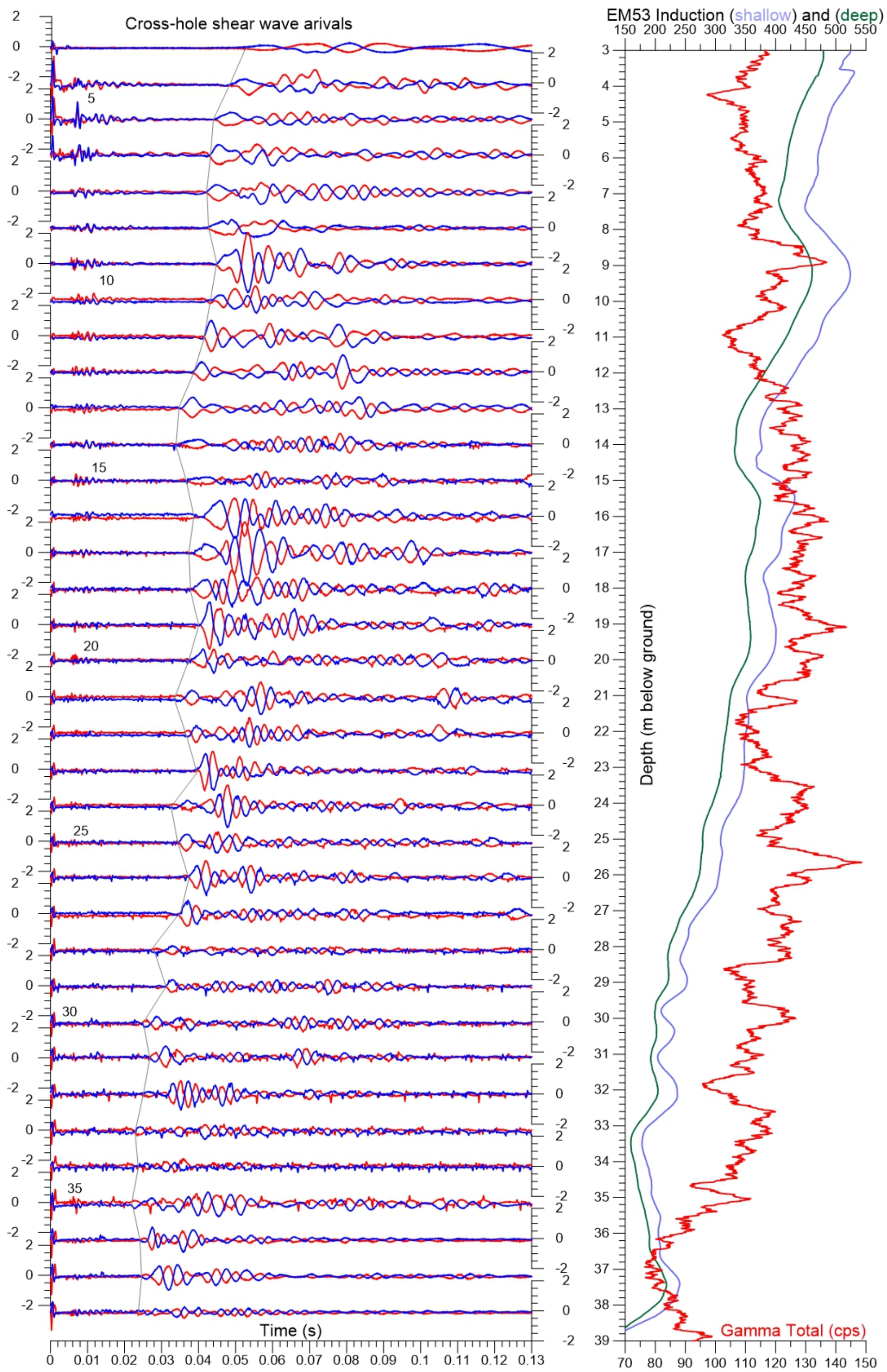

Figure 5. Profile of the vertical component cross-hole survey results at Cattle Lane arranged alongside with the gamma-ray activity and electromagnetic borehole logs

served a sandy layer in the bore during construction. Core recovery over this interval was very poor and good core only recommenced at 16.5 m. The age of sediments at this depth is approximately 55 to 60 ka *Acworth et al.* [2015] and correlates with *lake full* conditions

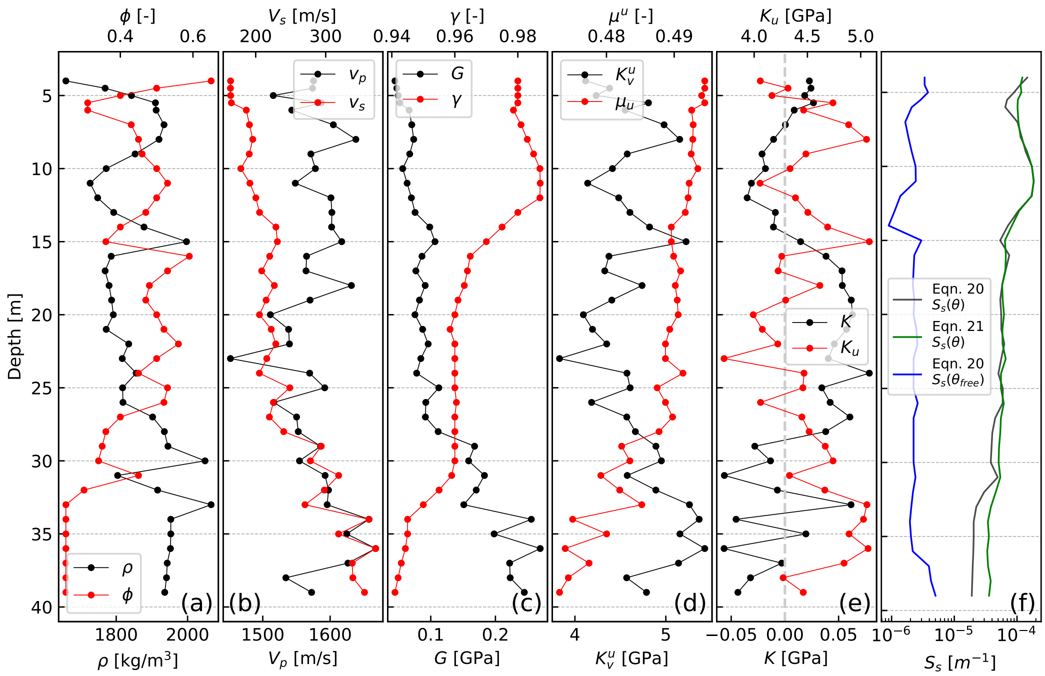

Figure 6. Depth profiles of the poroelastic parameters at the Cattle Lane Field Site (a) Porosity and density (b) Seismic velocities (c) Loading efficiency and shear modulus (d) Poisson's ration (undrained) and bulk modulus (vertically constrained and undrained) (e) Undrained vertical bulk modulus and undrained bulk modulus (f) Specific storage, quantified using Equation 20 assuming a measured bulk moisture content as total porosity θ (black line) and using Equation 21 with measured formation densities (green line). For smectite clays we assumed that $\alpha = 1$. For comparison, S_s calculated from the free water fraction $S_s(\theta_{free})$ is shown.

across eastern Australia [*Bowler*, 1990] as well as a period of increased dust concentration in Antarctic ice-cores [*Petit et al.*, 1999]. Shear waveforms remain stronger between 16 and 21 m depth (65 to 80 ka) during a time of reduced dust and higher temperatures. It is evident that the seismic shear waves could be further analyzed for an improved correlation with lithology.

A solid-grain modulus for the smectite dominated clay at the Cattle Lane Site is also required to mathematically constrain the poroelastic relationships. However, no data are available for Cattle Lane and we have not found values for smectite dominated clay in the literature. This is not surprising as the parameter is intrinsically difficult to measure given the fact that a high proportion of the water associated with the clay is adsorbed. Separating the clay from the water changes the material matrix. *Prasad et al.* [2001] directly measured Young's modulus and Poisson's Ratio of clay minerals and found values of $E_s = 5.9\,GPa$ and $\mu_s = 0.3$. These values can be converted to a clay solid gain modulus $K_s \approx 4.9$ GPa (Equation 7). However, this result leads to negative and therefore physically unrealistic values of K when Equation 24 is used. We hypothesize that the assumed linearity inherent to poroelastic theory breaks down for clays, a fact that has been noted before [*Bathija*, 2000]. We therefore make the reasonable assumption that $K_s \gg K$ and that the *Biot-Willis* coefficient $\alpha = 1$ for smectite clays.

The cross-hole survey results for Cattle Lane are shown in Figure 6b. Note that this is accompanied by existing depth specific total moisture (porosity) and bulk density provided by laboratory measurements in Figure 6a [*Acworth et al.*, 2015]. Again, the depth profiles of specific storage were calculated using Equations 20 and 21 with measured and estimated (interpolated) values of θ and ρ.

Our new method for calculating specific storage (Equation 21) relies on an estimate of the formation bulk density, whereas Equation 20 necessitates knowledge of the total porosity. The excellent match between both results confirms the accuracy of our laboratory based measurements from the core reported in *Acworth et al.* [2015]. These density and moisture content profiles were interpolated between field laboratory measurements for the clays at Cattle Lane to estimate values at the depths of the seismic measurements. An extended density formulation was required for the clay sites as it was not possible to use Equation 16 to replicate the higher bulk densities measured in the core samples. In recognition of the fact that much of the total moisture (θ) is adsorbed into the clay matrix, Equation 16 was extended to include a fraction of the total moisture as adsorbed moisture with a higher density [*Martin*, 1960; *Galperin et al.*, 1993] as follows:

$$\rho = \rho_s(1-\theta) + \rho_{ads}\theta_{ads} + \rho_w\theta_{free}, \tag{25}$$

where θ is the field measured moisture content, θ_{ads} is the adsorbed moisture fraction, and $\theta_{free} = \theta - \theta_{ads}$ is the free-water fraction; ρ_s is the solid density (between $2,000$ and $2,700\,kg/m^3$based upon published values), ρ_{ads} is the adsorbed water density (between $1,000$ and $1,400\,kg/m^3$) [*Martin*, 1960; *Galperin et al.*, 1993]. We note that the value of θ_{free} represents the water that can freely drain from the formation and is considered similar to the specific yield S_y value that would occur when the system becomes unconfined. With this approach, predicted values of density could be found that matched the observed natural densities by using an adsorbed water density of $1,400\,kg/m^3$. The intervening depths were then estimated using the determined range of values.

Water adsorbed onto clay minerals is recognized as having physical properties more akin to the solid than the fluid with considerable viscosity, elasticity and shear strength [*Galperin et al.*, 1993]. Considerable uncertainty concerns the physical properties of adsorbed water in the literature and its implications for groundwater resources or geotechnical understanding are unknown. Our results demonstrate that the response of clays and adsorbed water to stress can be fully explained by poroelastic theory using the total moisture content. This is to be expected because seismic waves and the loading efficiency stresses must act upon the total mass present. However, predicted specific storage values calculated using poroelastic theory assuming porosity is equal to the total water content will likely lead to large overestimates. This is because, as Equation 25 indicates, only a very limited proportion of the water present in the clays - that which is not adsorbed to the clay mineral structure - will be free to flow in and out of the pores and therefore contribute to the specific storage value. We calculate this quantity from the theoretical analysis of density (Equation 25). We note that the very low values of free-water porosity are corroborated by the field observation that the cores were almost dry to touch with little free water noted [*Acworth et al.*, 2015].

Our estimates of the free water in the clays (θ_{free}) are shown in Table 1 and have been used to re-evaluate the possible range of specific storage values via Equation 11. The results are shown by the blue line in Figure 6f and demonstrate that realistic values of specific storage for smectite clays are approximately $2 \cdot 10^{-6}\,m^{-1}$ consistent with previous work by *Acworth et al.* [2017, Table 1].

3.2 Analysis of the poroelastic parameter space for specific storage and its limits

We analyze the influence of the parameters involved in predicting specific storage using Equation 21 while aiming to better understand the interplay of the various components across the spectrum of consolidation found in real environments. Equation 21 relies only on three parameters, the undrained vertical bulk modulus K_v^u, the loading efficiency LE and the

Biot-Willis coefficient α. We also investigate the sensitivity to LE and α when Equation 21 is made independent of physical constants, i.e. $S_s^n = S_s \cdot K_u^v \cdot g \cdot \rho_w$.

We used the published poroelastic parameters for marble ($\alpha = 0.19$ [-]; $K = 40$ GPa; $K_u = 44$ GPa and $G = 24$ GPa) reported in [*Wang*, 2000, Table C.1] which is represents the most consolidated conditions measured in the literature. The undrained vertical bulk modulus K_v^u was derived using Equation 13. To represent unconsolidated conditions, we used the results presented earlier (Section 3.1). In our analysis, we assume that the loading efficiency can be calculated with good accuracy using the objective method of the groundwater response to atmospheric tides developed by *Acworth et al.* [2016a] and we allow values to vary between $0 \leq LE \leq 1$.

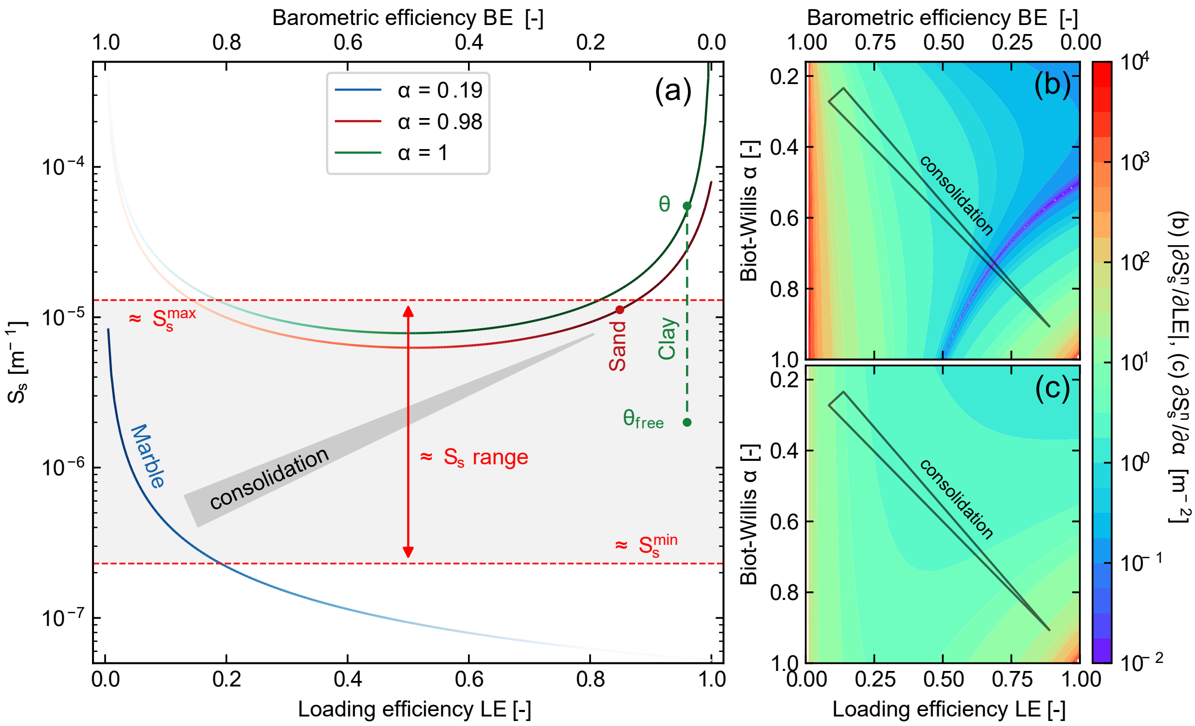

Figure 7. (a) Theoretical values of specific storage S_s as calculated using Equation 21 with literature values representative for the most consolidated system as well as our results representative for unconsolidated cases; (b) Sensitivity of specific storage to the loading efficiency LE, and (c) to the *Biot-Willis* coefficient α.

Figure 7a shows theoretical values of specific storage calculated using Equation 21 and the aforementioned parameter combinations, whereas Figures 7b and 7c illustrate the sensitivity of specific storage to changes in loading efficiency and the *Biot-Willis* coefficient, respectively. Note that only parts of this parameter space are reflective of real-world conditions, as is discussed in the following.

It is interesting that S_s is most sensitive to LE (Figure 7b) when this parameter assumes very high or very low values. For $\gamma \rightarrow 0$ the specific storage values obtained from Equation 21 diverge and are infinitely sensitive to loading efficiencies that are either very small ($LE \rightarrow 0$) or large ($LE \rightarrow 1$). Because diverging values of S_s are physically impossible, it can be deduced that a lower bound for loading efficiency must exist such that $LE > 0 \gamma > 0$ ($BE < 1$), and for values of $\alpha \rightarrow 1$ also $LE < 1 \gamma > 0$ ($BE > 0$). The sensitivity of specific storage to α appears to change for high values of loading efficiency (Figure 7c), such as is characteristic of water-saturated clays (Figure 7a). As such, elastic clay represents the most unconsolidated end-member with $\alpha = 1$.

While measurements of K_v^u exist in the literature for different materials [*Palciauskas and Domenico*, 1989; *Domenico and Schwartz*, 1997; *Wang*, 2000], little is known about how LE and α relate to real-world conditions. The *Biot-Willis* coefficient α describes the inverse of the ratio between bulk compressibility and grain compressibility [*Wang*, 2000]. Here, bulk compressibility values are correlated with the ability of the formation to reduce in volume when stressed, and the micro-scale mechanism is attributed to a rearrangement of individual grains [*Wang*, 2000]. It is interesting to note that under consolidated conditions, i.e. when the grains are locked together by chemical precipitate, the possibility of this rearrangement is much smaller than when compared to unconsolidated conditions, for which potential grain movement depends on the degree of packing. This is reflected in literature values of α, e.g. for marble the ratio of solid grain compressibility is high in relation to that of the formation ($\alpha = 0.19$) whereas for clay this is very small ($\alpha = 1$).

The loading efficiency describes the sharing of stress induced by the weight acting on a confined groundwater system. Barometric efficiency BE and loading efficiency LE describe the relative share of stress supported by the matrix and the groundwater [*Domenico and Schwartz*, 1997; *Wang*, 2000]. To date, relationships between its value and field conditions have not been well-described in the literature. It is interesting to note that in consolidated systems (e.g., marble or limestone) the stress can be absorbed mainly by the solid matrix and therefore $LE \rightarrow 0$ ($BE \rightarrow 1$). Such formations are thought to act as a barometer where the pore pressure is negatively correlated with the atmospheric pressure [*Meinzer*, 1928; *Jacob*, 1940; *Domenico and Schwartz*, 1997]. Contrarily, in unconsolidated systems where the stress is shared between water and matrix, the loading efficiency $LE \rightarrow 1$. Interestingly, *Acworth et al.* [2016a] found that $LE \approx 0.02$ ($BE \approx 0.98$) in a clayey-sand formation that existed beneath over-consolidated clays of Tertiary age at Fowlers Gap in western NSW [*Acworth et al.*, 2016b]. Again, this points to the fact that both γ and α can depend on how well grains are packed. An optimum packing will result in less individual grain movement and vice versa. It is therefore very difficult to determine a definitive relationship between all parameters involved. However, there appears to be an interrelated correlation for consolidation, here defined as optimum packing or grains locked in place by chemical precipitate, where $\alpha \rightarrow 0.2$ and $LE \rightarrow 0$ reflect more consolidated environments (see annotation in Figure 7). Further evaluation of BE and α for different environments will lead to improved understanding of these relationships.

We further apply these considerations to finding realistic bounds for specific storage. From Figure 7a, a hypothetical minimum specific storage can be deduced for the poroelastic parameters that characterize marble by following the blue line. However, the required loading efficiency of $LE \rightarrow 1$ is unrealistic as LE must remain towards the lower end. While a realistic bound is difficult to determine, we assume that for marble or limestone $LE \lesssim 0.2$. This results in a lower bound of $S_s^{min} \approx 2.3 \cdot 10^{-7}\, m^{-1}$ but which must be prone to considerable uncertainty.

On the other end, clays are generally thought of as having the highest values of specific storage due to their high compressibility [e.g., *Domenico and Schwartz*, 1997; *Fetter*, 2001]. Our results demonstrate that the total moisture content responds to stress and that poroelastic theory is able to quantify parameters for unconsolidated conditions. While this allows hypothetical estimates of S_s^{max}, our results further demonstrate that such values may not be meaningful to predict the quantity of water that is freely expelled from the clay, i.e. as is the case during groundwater pumping. It is well known that a large proportion of the total moisture content associated with a swelling clay is adsorbed water that is not readily released by simple drainage [*Jury et al.*, 1991; *Galperin et al.*, 1993]. The complicated nature of the interaction between water and clay minerals may also thwart the assumption of linearity inherent to poroelastic theory [*Bathija*, 2000]. It is therefore questionable whether poroelastic theory can determine an absolute upper bound S_s^{max} that is meaningful for water resources.

For our smectite clays, we estimate a maximum $S_s^{max}(\theta_{free}) \approx 1 \cdot 10^{-6}\, m^{-1}$ from values that are quantified in Figure 6, and a previous description by *Acworth et al.* [2017]. However, it appears that fine sands can have higher S_s values compared to clays (compare Figures 6 and 4). While it is difficult to estimate an upper limit for extractable water, this must be based on the free water fraction and we estimate this value to be maximal at $S_s^{max}(\theta_{free}) \approx 1.3 \cdot 10^{-5}$ (Figure 7a) for silts or kaolinitic dominated clays where the adsorbed water fraction is lower than in smectite dominated clays [*Jury et al.*, 1991].

Notably, both cross-hole seismic and tidal analysis yield coefficients representative of undrained conditions. The specific storage Equations 11 and 21 contain the drained bulk K and solid grain moduli K_s. Because both parameters are unknown, the poroelastic system remains mathematically unrestrained, i.e. not all parameters can be quantified by combining cross-hole seismics and tidal analysis. However, the unknown moduli occur as the *Biot-Willis* coefficient α (Equation 10) in Equations 21 and 24. As discussed here, values for unconsolidated bulk moduli are generally much lower compared to consolidated formations [*Domenico and Schwartz*, 1997; *Wang*, 2000]. This means that $K \ll K_s$ and therefore $K/K_s \rightarrow 0$ hence $\alpha = 1$, which leads to the following simplification of Equations 21 and 24 [*Wang*, 2000]

$$S_s = \rho_w g \frac{1}{K_v^u LE(1 - LE)} \tag{26}$$

and

$$K = K^u(1 - B) = \left(K_v^u - \frac{4}{3}G\right)\left(1 - 3LE\frac{1 - \mu^u}{1 + \mu^u}\right). \tag{27}$$

Equations 26 and 27 mathematically constrain the parameter space and can therefore be used to approximate the poroelastic properties of unconsolidated formations using cross-hole seismic surveys and the groundwater response to atmospheric tides.

We note here that our analysis also produces a value of the drained bulk modulus (K) from Equation 24 or Equation 27 although, for the sake of brevity, the value of these estimates for geotechnical investigations will be described in a subsequent paper.

3.3 Implications for groundwater resource analysis and modeling

The uncertainty and lack of groundwater storage properties on a global scale [*Richey et al.*, 2015] has meant that groundwater models generally use crude estimates of this parameter and also relegated it to a second-order importance. Even in aquifer testing interpretation, an order of magnitude estimate is often considered satisfactory [e.g. *Kruseman and de Ridder*, 1990]. This is despite the fact that this also implies a high degree of uncertainty in the derived transmissivity value since these parameters appear together in commonly used *Well Functions* via the relationships for aquifer hydraulic diffusivity, $D = T/S = K/S_s$. Thus the accuracy of transmissivity and storage terms are inextricably linked.

Hsieh et al. [1988] consider the accuracy of specific storage values calculated theoretically to only ± 50%. Such difficulty in obtaining representative aquifer storage values has meant that groundwater modeling has focused far more on transmissivity when trying to achieve satisfactory model calibration. The significance of variation in storage is almost always overlooked, despite the fact that variation in storage can have just as great an impact on predicted groundwater elevations.

From the perspective of hydrogeology, which is mostly concerned with the continuous extraction of water from the subsurface, the poroelastic definitions *drained* and *undrained* (see Section 2.1) change over time. As water is removed from a bore, clearly there is a change in mass occurring and $d\zeta/dt = Q\rho_w$, where Q is the volume of water abstracted. However, after a long time period of pumping from a confined aquifer, the system reaches steady-state [*Kruseman and De Ridder*, 2000] and is at constant pore pressure ($dp/dt = 0$) as well as mass ($d\zeta/dt = 0$). By the poroelastic definitions given in Section 2.1, stress conditions become drained as soon as extraction starts but transition into undrained conditions when steady-state is reached. Drained and undrained elastic parameters can therefore be thought of as bounds for the poroelastic conditions encountered as a result of pumping.

A more complete consideration of poroelastic theory, as was undertaken in this paper, illustrates that the specific storage is limited to $2.3 \cdot 10^{-7}\, m^{-1} \lessapprox S_s \lessapprox 1.3 \cdot 10^{-5}\, m^{-1}$ with the lower limit derived from the poroelastic parameters of marble and the upper limit for materials where the grain size is smaller than that of fine sands but where the adsorbed water fraction is small compared to the total water content.

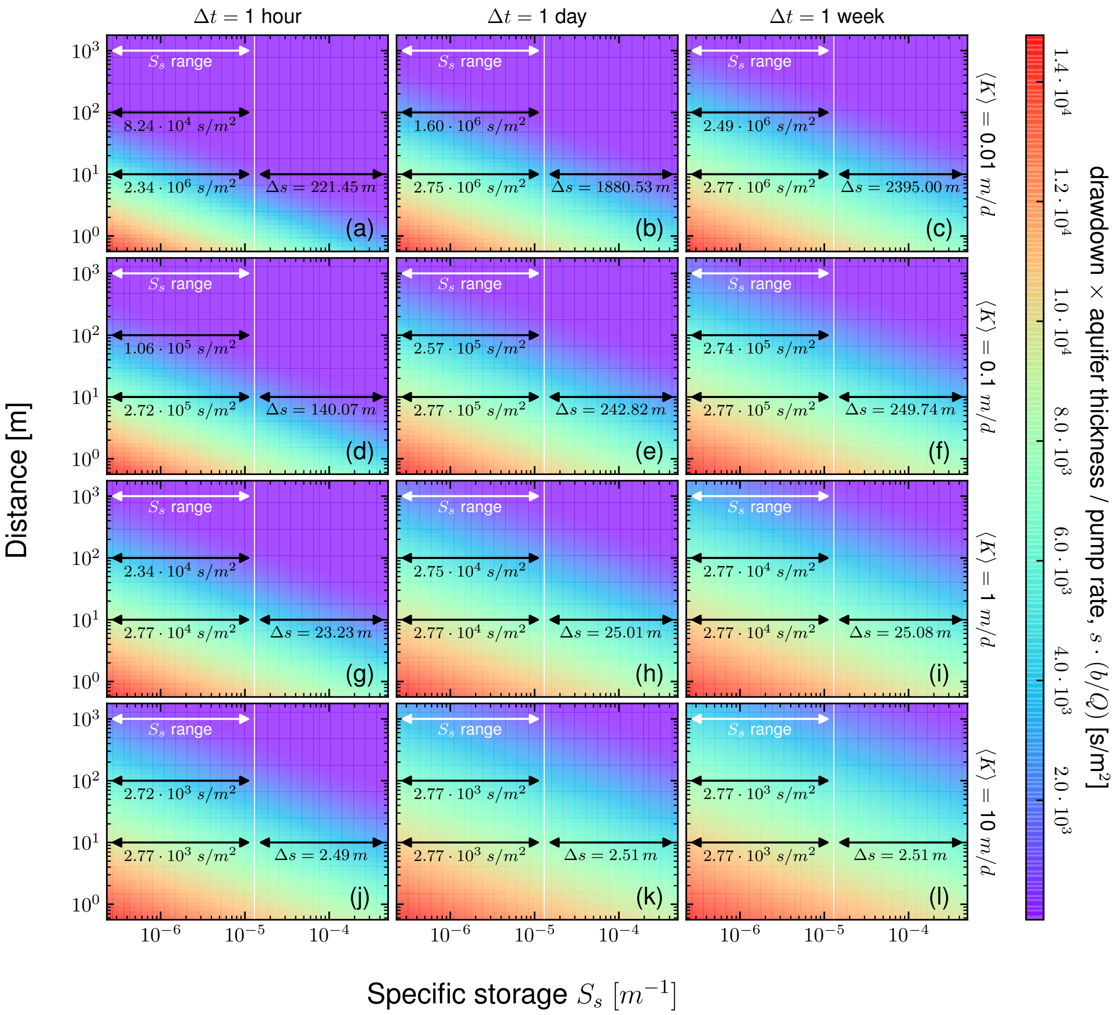

Figure 8. Normalised drawdown [s/m^2] (i.e., Groundwater head drawdown (s) × aquifer thickness (b) / pump rate (Q)) for a confined aquifer as calculated using the solution by *Theis* [1935]. To convert to drawdown in meters, multiply the values by Q/b. Notation on the left shows generic drawdown differences across the possible specific storage values of $2.3 \cdot 10^{-7}\, m^{-1} \lessapprox S_s \lessapprox 1.3 \cdot 10^{-5}\, m^{-1}$. Notation on the right illustrates our field example (Δs) across the possible specific storage values assuming our upper limit of S_s for discrete times, distances and hydraulic conductivities as well as a pumping rate of $Q = 50\, L/s$ and an aquifer thickness of $b = 50\, m$.

The uncertainty in S_s is substantial for estimating the drawdown caused by pumping. To illustrate the maximum possible drawdown difference due to our range in specific storage, Figure 8 shows the drawdown normalized by pumping rate and aquifer thickness for discrete pumping durations and realistic aquifer hydraulic conductivities ($\langle K \rangle$ = 0.01, 0.1, 1, 10 m/d) estimated using the standard *Theis* [1935] solution. Interestingly, it appears that the difference in normalized drawdown across the range of S_s is independent of the distance to the pumped well for high conductivities (Figure 8j-l) or long extraction periods (Figure 8f,i,l).

Where a groundwater model has performed a satisfactory mass balance using a very high storage coefficient, but we accept that such a value is not realistic based upon the known properties of the formation and the poroelastic theory described earlier, then we are forced to recognize that a large proportion of the water delivered can not come from storage changes within the formation. This must lead to a re-evaluation of the conceptual model of an aquifer and the inclusion of effective leakage into the modeled space, for example either from upwards or downwards leakage through bounding aquitards or from lateral movement from channels associated with rivers or other recharge boundaries.

At our field sites, especially on the Liverpool Plains, uncertainty regarding specific storage persists in modeling groundwater resources where new coal mines are proposed, and there is a possibility of future coal-seam gas extraction. As very few, if any, measurements of specific storage in the low permeability units are available from pumping test studies, values of specific storage in the range of $1 \cdot 10^{-6} m^{-1} \leq S_s \leq 5 \cdot 10^{-4}\, m^{-1}$ have been used to allow groundwater level calibration [*McNeilage*, 2006; *Price and Bellis*, 2012]. While the lower end is similar to values we have calculated from poroelastic analysis (an average of $\approx 2 \cdot 10^{-6}\, m^{-1}$), the upper value is at least an order of magnitude too high. The worst case difference in drawdown resulting from lowering S_s to the upper bound determined here would be $\Delta s \approx 25\, m$ at a distance of 10 m from the extraction bore, assuming a hydraulic conductivity of $\langle K \rangle = 1\, m/d$, constant rate pumping $Q = 50\, L/s$, aquifer thickness of $b = 50\, m$ (Figure 8g-i). Our analysis supports the observations of rapid downward leakage in response to pumping on the Liverpool Plains [*Timms and Acworth*, 2004; *Acworth and Timms*, 2009].

Our findings have global implications wherever groundwater models have been calibrated using values of specific storage that are unrealistically high ($\gg 1.3 \cdot 10^{-5}\, m^{-1}$). We should of course add the caveat that our poroelastic analysis is based upon the theory of linear poroelasticity and assumes perhaps an unwarranted degree of material homogeneity. However, use of the assumption that the *Biot-Willis* coefficient is unity will address this uncertainty. We anticipate that our results will help improve conceptual models that are used to quantify aquifer parameters for groundwater resource estimates and management.

4 Conclusions

We have derived new equations which relate the drained and undrained poroelastic parameters governing specific storage in consolidated materials, incorporating the effects of both solid grain and bulk compressibility. We have shown how the necessary parameters can be derived from a combination of cross-hole seismic surveys and high frequency groundwater level measurements, reducing the large uncertainty that is normally inherent in storage estimates using a priori estimations of such parameters. Our new method for estimating specific storage relies on an estimation of formation density. However, this is relatively easy to constrain in comparison with the assumptions inherent in other methods e.g. reliance of porosity values for tidal analysis [*Acworth et al.*, 2016a] or the conceptual or numerical simplifications applied during pumping test inversion [*Kruseman and De Ridder*, 2000].

We have presented field data and analysis to demonstrate the applicability of the new method in the context of two contrasting lithologies (sand, and smectite clay) and the results show excellent agreement with those derived from an alternative method. Our results yield a new constraint of $S_s \lessapprox 1.3 \cdot 10^{-5}\, m^{-1}$ for the physically plausible upper boundary of specific storage for unconsolidated materials, applicable as long as the adsorbed water fraction is small compared to the total water content. For clay-rich formations with substantial adsorbed water, specific storage will be much lower than this value (as shown in Figure 6) but in a range that is only as certain as the estimation of the free water content will allow. This occurs because the adsorbed water significantly contributes to the compressibility of the formation, but because it cannot flow under an imposed hydraulic gradient it thus does not contribute to available groundwater storage .

It is common for literature values of specific storage of aquifers to be above the theoretical maximum we present here. Where this is the case, a re-appraisal of the conceptual model and data that have been used to derive such values is needed. This is critical to ensure more robust management of groundwater resources from confined aquifers or to predict the possible subsidence due to continued groundwater abstraction, issues of increasing importance worldwide.

Acknowledgments

The dataset for this work is freely accessible on *ResearchGate* (`https://dx.doi.org/10.13140/RG.2.2.31853.28646`). The Cattle Lane site was partly constructed using funding supplied by the *National Centre for Groundwater Research and Training (NCGRT)*, an Australian Government initiative supported by the *Australian Research Council* (*ARC*) and the *National Water Commission* (*NWC*). The data used in this analysis was collected with equipment provided by the Australian Federal Government financed *National Collaborative Research Infrastructure Strategy* (*NCRIS*). The groundwater data is available through the *NCRIS Groundwater Database*: `http://groundwater.anu.edu.au`. We acknowledge the excellent *Matplotlib v2.1.2* library [*Hunter*, 2007] which was used to generate most of the figures. GCR was partly supported by the *NCGRT*. LJSH was partly supported by the *Swiss National Science Foundation (SNF/FNS)*, project 166233. Funding is gratefully acknowledged by MOC for an Independent Research Fellowship from the UK Natural Environment Research Council (NE/P017819/1). We thank Dayna McGeeney for conducting the core moisture and density analyses, and Hamish Studholme for supervising the drilling and coring work.

Appendix

Variable	Definition and SI Units
ads	(subscript) Adsorbed water
$free$	(subscript) Free water
s	(subscript) Solid matrix
w	(subscript) Water
v	(subscript) Vertical
h	(subscript) Horizontal
u	(superscript) Undrained
$< none >$	(superscript) Drained
B	*Skempton* coefficient [-]
BE	Barometric Efficiency [-]
$E^{(u)}$	Young's Modulus [Pa]
g	Acceleration due to gravity [m/s^2]
G	Shear (or rigidity) modulus [Pa]
$K_{(s)}^{(u)}$	Modulus of elasticity [Pa]
$K_{(h,v)}^{(u)}$	Uniaxial (horizontal or vertical) or confined modulus of elasticity [Pa]
l	Length [m]
LE	Uniaxial loading efficiency [-]
M_2^{ET}	M_2 Earth tide amplitude^a [m/s^2]
M_2^{GW}	M_2 Groundwater amplitude^a [m H_2O or Pa]
p	Pressure [Pa]
h	Groundwater head [m]
S_s	Specific storage [m^{-1}]
S_y	Specific yield [-]
S_2^{AT}	S_2 Atmospheric tide amplitude^a [m H_2O or Pa]
S_2^{ET}	S_2 Earth tide amplitude^a [m/s^2]
S_2^{GW}	S_2 Groundwater amplitude^a [m H_2O or Pa]
V	Volume [m^3]
V_p	Seismic P-wave velocity [m/s]
V_s	Seismic S-wave velocity [m/s]
α	*Biot-Willis* coefficient [-]
$\beta_{(v,s)}^{(u)}$	Compressibility [Pa^{-1}]
$\Delta\phi$	Phase shift [rad]
ϵ	Strain [Pa^{-1}]
$\lambda^{(u)}$	Lamé's modulus [-]
$\mu^{(u)}$	Poisson's Ratio [-]
ρ	Bulk density [kg/m^3]
σ	Stress [Pa]
θ	Total porosity (= water content in saturated zone) [-]
z	Depth [m]
s	Change in head with pumping (drawdown) [m]
b	Aquifer thickness [m]
$\langle K \rangle$	Hydraulic conductivity [m/s]
Q	Pumping rate [m^3/s]

Table 2. Definitions of variables used. ^{a} See *Acworth et al.* [2016a].

References

Acworth, R. (2007), Measurement of vertical environmental-head profiles in unconfined sand aquifers using a multi-channel manometer board, *Hydrogeology Journal*, *15*(7), 1279–1289, doi:10.1007/s10040-007-0178-9, first Online: 13 April 2007.

Acworth, R., and J. Jankowski (1993), Hydrogeochemical zonation of groundwater in the botany sands aquifer, sydney, *AGSO Journal of Australian Geology*, *14*(2), 193–200.

Acworth, R., and L. Jorstad (2006), Integration of multi-channel piezometry and electrical tomography to better define chemical heterogeneity in a landfill leachate plume within a sand aquifer, *Journal of Contaminant Hydrology*, *83*(3-4), 200–220, doi:10.1016/j.jconhyd.2005.11.007.

Acworth, R., and W. Timms (2009), Evidence for connected water processes through smectite-dominated clays at breeza, new south wales, *Australian Journal of Earth Sciences*, *56*(1), 81–96, doi:10.1080/08120090802541952.

Acworth, R., W. Timms, B. Kelly, D. McGeeney, T. Ralph, Z. Larkin, and G. Rau (2015), Late Cenozoic paleovalley fill sequence from the southern Liverpool Plains, New South Wales - implications for groundwater resource evaluation, *Australian Journal of Earth Sciences*, *62*, 657–680, doi:10.1080/08120099.2015.1086815.

Acworth, R., L. Halloran, G. Rau, M. Cuthbert, and T. Bernadi (2016a), An objective method to quantify groundwater compressible storage using earth and atmospheric tides, *Geophysical Research Letters*, *43*(22), 11,671–11,678, doi:10.1002/2016gl071328, submitted 27 September 2016.

Acworth, R., G. Rau, M. Cuthbert, E. Jensen, and K. Leggett (2016b), Long-term spatio-temporal precipitation variability in arid-zone australia and implications for groundwater recharge, *Hydrogeology Journal*, *24*(4), 905–921.

Acworth, R. I., G. C. Rau, L. J. Halloran, and W. A. Timms (2017), Vertical groundwater storage properties and changes in confinement determined using hydraulic head response to atmospheric tides, *Water Resources Research*, *53*(4), 2983–2997, doi:10.1002/2016WR020311.

Alley, W. M., R. W. Healy, J. W. LaBaugh, and T. E. Reilly (2002), Flow and storage in groundwater systems, *Science*, *296*, doi:10.1126/science.1067123.

Bathija, A. P. (2000), Elastic properties of clays, Ph.D. thesis, Colorado School of Mines.

Biot, M. (1941), General theory of three-dimensional consolidation, *Journal of Applied Geophysics*, *12*, 155–164.

Bowler, J. (1990), The last 500,000 years, in *The Murray*, edited by N. Mackay and D.Eastburn, pp. 95–104, The Murray-Darling Basin Commission, The Murray-Darling Basin Commission, Canberra, Australia.

Bredehoeft, J. D., and R. L. Cooley (1983), Comment on “a note on the meaning of storage coefficient by T. N. Narasimhan and B. Y. Kanehiro", *Water Resources Research*, *19*(6), 1632–1634, doi:10.1029/WR019i006p01632.

Clayton, C. (2011), Stifness at small strain: research and practice, *Geotechnique*, *61*(1), 5–37, doi:10.1680/geot.2011.61.1.5.

Cooper, H. (1966), The equation of groundwater flow in fixed and deforming coordinates, *Journal of Geophysical*, *71*(20), 4785–4790, doi:10.1029/JZ071i020p04785.

Crice, D. (2011), Near-surface, downhole shear-wave surveys: A primer, *The Leading Edge: GEOPHYSICS*, pp. 164–171.

David, K., W. Timms, S. Barbour, and R. Mitra (2017), Tracking changes in the specific storage of overburden rock during longwall coal mining, *Journal of Hydrology*, *553*, 304 – 320, doi:https://doi.org/10.1016/j.jhydrol.2017.07.057.

Davis, A. (1989), Determination of dynamic elastic parameters from crosshole testing, *Scientific Drilling*, *1*(1), 54–62.

Davis, A., and D. Taylor-Smith (1980), Dynamic elastic moduli loging of foundation materials, in *Offshore Site Investigation*, edited by D. Ardus, Graham and Trotman, pages 21-132.

Domenico, P. (1983), Determination of bulk rock properties from ground-water level fluctuations, *Environmental and Engineering Geoscience*, (3), 283–287, doi:10.2113/gseegeosci.xx.3.283.

Domenico, P., and F. Schwartz (1997), *Physical and Chemical Hydrogeology*, 2nd ed., John Wiley and Sons.

Fetter, C. (2001), *Applied Hydrogeology*, fourth ed., Prentice Hall, Upper Saddle River, New Jersey 07458, USA.

Galperin, A., V. Zaytsev, A. Yu, and Y. Norvatov (1993), *Hydrogeology and Engineering Geology*, A.A. Balkema, Rotterdam, translated from Russian and edited by R.B. Zeidler of H*T*S*, Gdańsk.

Gleeson, T., W. M. Alley, D. M. Allen, M. A. Sophocleous, Y. Zhou, M. Taniguchi, and J. VanderSteen (2012), Towards sustainable groundwater use: setting long-term goals, backcasting, and managing adaptively, *Groundwater*, *50*(1), 19–26, doi:10.1111/j.1745-6584.2011.00825.x.

Green, D., and H. Wang (1990), Storage as a poroelastic coefficient, *Water Resources Research*, *26*(7), 1631–1637, doi:10.1029/WR026i007p01631.

Hantush, M. S. (1960), Modification of the theory of leaky aquifers, *Journal of Geophysical Research*, *65*(11), 3713–3725, doi:10.1029/JZ065i011p03713.

Hantush, M. S. (1967a), Flow of groundwater in relatively thick leaky aquifers, *Water Resources Research*, *3*(2), 583–590, doi:10.1029/WR003i002p00583.

Hantush, M. S. (1967b), Flow to wells in aquifers separated by a semipervious layer, *Journal of Geophysical Research*, *72*(6), 1709–1720, doi:10.1029/JZ072i006p01709.

Hsieh, P. A., J. D. Bredehoeft, and S. A. Rojstaczer (1988), Response of well aquifer systems to earth tides: Problem revisited, *Water Resources Research*, *24*(3), 468–472, doi:10.1029/WR024i003p00468.

Hunter, J. D. (2007), Matplotlib: A 2d graphics environment, *Computing In Science & Engineering*, *9*(3), 90–95, doi:10.1109/MCSE.2007.55.

Jacob, C. (1940), On the flow of water in an elastic artesian aquifer, *Transactions American Geophysics Union*, *21*(2), 574–586, doi:10.1029/TR021i002p00574.

Jury, W., W. Gardner, and W. Gardner (1991), *Soil Physics*, fifth ed., John Wiley & Sons, inc.

Kruseman, G., and N. de Ridder (1990), Analysis and evaluation of pumping test data, *Publication 47*, International Institute for Land Reclamation and Improvement, P.O. Box 45, 6700 AA Wageningen, The Netherlands, 1994, Second Edition (Completely Revised).

Kruseman, G., and N. De Ridder (2000), *Analysis and Evaluation of Pumping Test Data*, vol. 47, 2nd edition ed., ILRI.

Martin, R. (1960), Adsorbed water on clay: A review, *Clays and Clay Minerals*, *9*(1), 28–70, doi:10.1346/CCMN.1960.0090104.

Mathews, M., V. Hope, and C. Clayton (1994), The geotechnical value of ground stiffness determined using seismic methods, in *Modern Geophysics in Engineering Geology, EGAC 94 - Proceedings of 30th Annual Conference of the Engineering Group of the Geological Society, University of Liege, Belgium, 1994*, pp. 7–12, The Geological Society of London.

McNeilage, C. (2006), Upper namoi groundwater flow model: Model development and calibration, *Tech. rep.*, Australian Government, New South Wales Department of Natural Resources.

Meinzer, O. E. (1928), Compressibility and elasticity of artesian aquifers, *Economic Geology*, *23*(3), 263–291, doi:10.2113/gsecongeo.23.3.263.

Narasimhan, T. (1979), The significance of the storage parameter in saturated-unsaturated groundwater flow, *Water Resources Research*, *15*(3), 569–576, doi:10.1029/WR015i003p00569.

Narasimhan, T. (1983), Reply, *Water Resources Research*, *19*(6), 1630–1640, doi:10.1029/WR019i006p01636.

Narasimhan, T., and B. Kanehiro (1980), A note on the meaning of storage coefficient, *Water Resources Research*, *16*(2), 423–429, doi:10.1029/WR016i002p00423.

Palciauskas, V., and P. Domenico (1989), Fluid pressures in deforming porous rocks, *Water Resources Research*, *25*(2), 203–213, doi:10.1029/WR025i002p00203.

Petit, J., J. Jouzel, D. Raynauld, J. M. Barkov, N.I.Barnola, I. Basile, M. Bender, J. Chappellaz, M. Davis, G. Delaygue, M. Delmotte, V. M. Kotlyakpv, M. Legrand, V. Lipenkov, C. Lorius, L. Pepin, C. Ritz, E. Saltzman, and M. Stievenard (1999), Climate and atmospheric history of the past 420,000 years from the Vostok ice core, Antarctica, *Nature*, *399*(3), 429–436.

Prasad, M., M. Kopycinska, U. Rabe, and W. Arnold (2001), Measurement of young's modulus of clay minerals using atomic force acoustic microscopy, *Geophysical Research Letters*, *29*(8), 13–1–13–4, doi:10.1029/2001GL014054.

Price, G., and L. Bellis (2012), Namoi cathchment water study - independent expert - final study report, *Tech. Rep. 50371/P4-R2 FINAL*, Schlumberger Water Services (Australia) Pty Ltd, department of Trade and Investment, Regional Infrastructure and Services, New South Wales, (DTIRIS NSW) Locked Bag 21 Orange NSW 2800 Australia.

Richardson, N., K. Williams, K. Briggs, and E. Thorsos (2002), Dynamic measurement of sediment grain compressibility at atmospheric pressure: acoustic applications, *IEEE Journal of Oceanic Engineering*, *27*(3), 593–601, doi:10.1109/JOE.2002.1040941.

Richey, A. S., B. F. Thomas, M.-H. Lo, J. S. Famiglietti, S. Swenson, and M. Rodell (2015), Uncertainty in global groundwater storage estimates in a total groundwater stress framework, *Water Resources Research*, doi:10.1002/2015WR017351.

Theis, C. (1935), The relationship between the lowering of the piezometric surface and the rate and duration of discharge of a well using groundwater storage, *Transactions American Geophysical Union*, *2*, 519–524.

Timms, W., and R. Acworth (2004), Induced leakage through aquitard fractures and windows - impacts on groundwater quality at irrigation sites, in *The 9th Murray-Darling Basin Groundwater Workshop 2004*.

Van Der Kamp, G., and J. Gale (1983), Theory of earth tide and barometric effects in porous formations with compressible grains, *Water Resources Research*, *19*(2), 538–544, doi: 10.1029/WR019i002p00538.

Verruijt, A. (2016), *Theory and Problems of Poroelasticity*, self published.

Wada, Y., L. P. H. v. Beek, N. Wanders, and M. F. Bierkens (2013), Human water consumption intensifies hydrological drought worldwide, *Environmental Research Letters*, *8*.

Wang, H. F. (2000), *Theory of Linear Poroelasticity with Applications to Geomechanics and Hydrogeology (Princeton Series in Geophysics)*, Princetown University Press.

Webb, S., and K. Watson (1979), Hydraulic behaviour of an unconfined aquifer, *Technical Paper 38*, Australian Water Resources Council, Australian Government Publishing Service, Canberra.